Effects of pressure on the structure and lattice dynamics of $TmPO_4$: Experiments and calculations

E. Stavrou,[1,2] A. Tatsi,[1,*] C. Raptis,[1] I. Efthimiopoulos,[2] K. Syassen,[2,†] A. Muñoz,[3] P. Rodríguez-Hernández,[3] J. López-Solano,[3] and M. Hanfland[4]

[1]*Department of Physics, National Technical University of Athens, GR-15780 Athens, Greece*

[2]*Max-Planck-Institut für Festkörperforschung, Heisenbergstraße 1, DE-70569 Stuttgart, Germany*

[3]*Departamento de Física Fundamental II, Instituto de Materiales y Nanotecnología, Universidad de La Laguna and MALTA Consolider Team, La Laguna ES-38205, Tenerife, Spain*

[4]*European Synchrotron Radiation Facility, FR-38043 Grenoble, France*

(Received 15 November 2011; published 23 January 2012)

Thulium phosphate ($TmPO_4$) with the tetragonal zircon-type structure has been studied using angle-dispersive powder x-ray diffraction and Raman spectroscopy in a diamond anvil cell up to 55 GPa (at room temperature). The results from both experimental methods reveal a pressure-induced structural phase transition from zircon to a scheelite-type structure at 20 GPa. At the same pressure, a second phase with the monazite structure is also formed at a low concentration, which decreases and eventually vanishes with increasing pressure. Our *ab initio* total-energy and lattice-dynamics calculations are in good agreement with experimental findings. The calculations indicate that the main transition to the scheelite structure is related with the softening of a silent B_{1u} mode. Upon decompression, $TmPO_4$ reverses back to the original zircon structure showing significant hysteresis. The results are discussed in relation to the observed general structural systematics and phase transition sequences in zircon-type APO_4 orthophosphates under pressure.

DOI: 10.1103/PhysRevB.85.024117 PACS number(s): 62.50.−p, 64.70.kp, 71.15.Nc, 78.30.Am

I. INTRODUCTION

Ternary compounds with the general formula ABX_4 ($X = O^{2-}$, F^-) crystallize in a variety of crystal structures. The structures can be classified in terms of ratios of the ionic radii r_A, r_B, and r_X.[1–5] Related two-dimensional (2D) structure maps using coordinates r_B/r_X and r_A/r_X and named after Bastide[4] have been helpful to demonstrate the systematics among ambient-pressure phases. The maps also provide an overall approximate guideline for phase transition sequences under high pressure. ABO_4 oxides come with combinations of cation coordination numbers ($z_A - z_B$) of (4-4), (6-4), (8-4), (12-4), and (6-6). When r_A is much larger than r_B, the B cations are always tetrahedrally coordinated by oxygen atoms.[3] The general trend under pressure is toward structures of increased cation coordination number.[3] Thus, the compounds will generally transform along the northeast direction in the Bastide diagram (see, e.g., Fig. 15 in Ref. 5). The structural behavior and the phase transition sequences under pressure of several families of ABO_4 compounds were summarized in Ref. 3. More recent experimental and theoretical results on pressure-induced phase transitions in ABO_4 compounds are reviewed in Ref. 5.

Orthophosphates APO_4 (A = trivalent metal) generally crystallize in either the tetragonal zircon-type [space group (SG): D_{4h}^{19} ($I4_1/amd$), $Z = 4$] or the closely related monoclinic monazite-type [SG: $C_{2h}^5(P2_1/n)$, $Z = 4$] structure, depending on the A^{3+} cation radius. Because of the small radius of the P^{5+} cation compared to that of the O^{2-} anion ($r_P \ll r_O$), orthophosphates occupy positions close to the base of Bastide's structure map.[4,5] The zircon structure (Fig. 1, top) consists of alternating PO_4 tetrahedra and AO_8 dodecahedra arranged in linear chains along the c axis.[6,7] Orthophosphates containing large A^{3+} cations tend to crystallize in the closely related monazite structure (Fig. 1 middle), where the A^{3+} cations adopt a ninefold coordination (with formation of AO_9 polyhedra). Relative to the zircon type, the PO_4 tetrahedra are rotated in monazite and (100) planes are shifted laterally.[6,7] In the case of the rare-earth orthophosphates RPO_4, those with a small R^{3+} size (the heavy ones R = Tb, Dy, Ho, Er, Tm, Yb, Lu) adopt the zircon-type structure at ambient conditions, whereas those with larger R^{3+} radius (R = La, Ce, Pr, Nd, Sm, Eu, Gd) crystallize in the monazite-type structure.[6,7] Some of the RPO_4 display metastability[8,9] (dimorphism) at ambient conditions. Specifically, depending on the growth conditions, $GdPO_4$, $TbPO_4$, $DyPO_4$, and $HoPO_4$ can adopt[9] either the zircon or the monazite structure.

The high-pressure behavior of either zircon- or monazite-type RPO_4 compounds was addressed only recently. High-pressure Raman studies[10,11] of zircon-type $TbPO_4$, lying close to the zircon-monazite border, showed a first-order phase transition at 9.5 GPa. The most likely structure for the high-pressure phase was proposed to be the monazite type, based on the resemblance of its Raman spectrum with that of the ambient-pressure spectrum of monazite-type $GdPO_4$. The zircon-to-monazite transition of $TbPO_4$ was confirmed in a study involving both x-ray diffraction and calculations.[12] Subsequently, zircon-to-monazite transitions were reported for YPO_4 (Refs. 13 and 14) and $ErPO_4$ (Ref. 14). However, other zircon-type RPO_4's, such as $YbPO_4$ (Ref. 15), $LuPO_4$ (Ref. 15), and $ScPO_4$ (Ref. 13) were found to undergo a transition to the scheelite structure [SG: $C_{4h}^6(I4_1/a)$, $Z = 4$] at 22, 19, and 30 GPa, respectively.

In this work, we are concerned with thulium phosphate, $TmPO_4$, which adopts the zircon-type structure at ambient conditions. The compound has attracted interest for its low-temperature elastic[16] and magnetic[17] properties. Specifically, $TmPO_4$ exhibits an anomalous softening of the shear elastic constant C_{66} (related with a B_{2g} lattice distortion) with decreasing temperature, showing a nonzero minimum at 20 K.[16] This anomalous trend has been attributed to Jahn-Teller

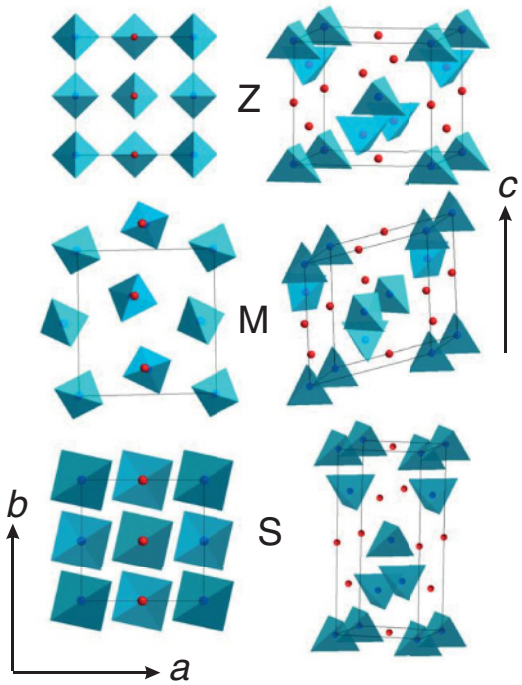

FIG. 1. (Color online) Tetragonal zircon-type (Z, top), monoclinic monazite-type (M, middle), and tetragonal scheelite-type (S, bottom) crystal structures of $TmPO_4$ plotted in two different styles. Projections down the respective c axes are shown on the left, and perspective views with the c axis oriented approximately vertically are shown on the right. To better illustrate the relative arrangement of PO_4 polyhedra, the origins of the unit cells are chosen at phosphorous positions.

interactions, which involve lattice modes and a splitting of the ground-state electronic level of the Tm^{3+} cation.[16] However, different from the isomorphic $TbPO_4$ (Ref. 18), the Jahn-Teller effect in $TmPO_4$ is not strong enough to induce a spontaneous magnetic ordering or a structural phase transition at low temperature.[16,17]

The size of the Tm^{3+} cation in $TmPO_4$ is intermediate between the respective cation sizes of the isomorphic $ErPO_4$ and $YbPO_4$ compounds. Under pressure, $ErPO_4$ undergoes a phase transition to monazite,[14] whereas $YbPO_4$ transforms to scheelite.[15] Therefore, it is appealing to investigate the transition sequence of $TmPO_4$ at high pressure to relate it to that of neighboring zircon-type rare-earth phosphates, and to compare with the recently proposed pressure-temperature phase diagrams of selected RPO_4 compounds.[19]

We report here a combined structural and lattice dynamics investigation of $TmPO_4$ under pressure involving synchrotron x-ray diffraction, Raman scattering, and *ab initio* total-energy and lattice-dynamics calculations. Both experimental and calculated results show that the high-pressure phase of $TmPO_4$ at room temperature has the scheelite structure. However, at the onset of the zircon-to-scheelite phase transition near 17–20 GPa, a metastable minority phase with the monazite structure is formed. The fraction of the monazite structure decreases and eventually vanishes with increasing pressure, thus leaving the scheelite-type modification as the stable high-pressure phase of $TmPO_4$. The high-pressure scheelite phase reverses back to the original zircon phase upon decompression to ambient pressure, but with a large hysteresis. A new aspect revealed by lattice-dynamics calculations is that the pressure-driven instability of the zircon phase may be related to the softening of a silent mode, which corresponds to rotational motions of PO_4 tetrahedra.

II. EXPERIMENTAL PART

A. Samples and methods

Flux-grown single crystals of $TmPO_4$ originating from the same batch as that in Ref. 20 were used for both x-ray diffraction and Raman measurements. For the diffraction experiments, the single-crystal samples were crushed and ground to a fine powder and then loaded into a diamond anvil cell. It is important to note that helium was used as the pressure-transmitting medium in order to ensure good hydrostaticity. A rectangular piece of single crystal, cut and polished along the crystallographic axes, was used for polarized Raman measurements at ambient pressure (see below for details). For the high-pressure Raman sessions, small single crystals of $TmPO_4$ with a typical dimension of $\sim$50 μm were loaded into a diamond anvil cell (DAC) with a mixture of methanol-ethanol-water in the volume ratio 16:3:1 as the pressure-transmitting medium. In both x-ray and Raman high-pressure experiments, a tiny sphere of ruby was also loaded into the anvil cell for monitoring the pressure through the shift of its R-line luminescence bands.[21]

Angle-dispersive powder x-ray diffraction data ($\lambda = 0.4147$ Å) were measured up to 54.6 GPa at room temperature at the ID09A beamline of the European Synchrotron Radiation, Grenoble, using image plate detection. The images were integrated using the FIT2D (Ref. 22) program to yield intensity versus 2θ diagrams.

High-pressure Raman experiments were performed in backscattering geometry up to 24 GPa at room temperature, using a single-stage grating spectrometer combined with a CCD detector (Labram). The spectral resolution was about 3 cm^{-1}. In order to assign the Raman modes of zircon-structured $TmPO_4$, polarized Raman measurements were performed at ambient conditions and in a 90° scattering geometry, using a SPEX double monochromator in combination with a cooled photomultiplier and an oriented single crystal. In all Raman experiments, the 514.5-nm line of an Ar^+ laser was used.

B. X-ray diffraction results and analysis

Figure 2 shows selected x-ray diffraction diagrams of $TmPO_4$ obtained at different pressures up to 54.6 GPa. Apart from pressure-induced shifts of the Bragg peaks, the diffraction pattern does not change significantly up to 17.6 GPa. All the observed peaks in this pressure range can be indexed as zircon type. At a pressure $P_c = 20.3$ GPa, new Bragg peaks appear, while existing peaks of the zircon phase become weaker (but not disappearing altogether), thus indicating the onset of a phase transition. At about 23 GPa, the zircon phase is not detectable any more. A set of new peaks marked with an asterisk in Fig. 2 can be readily indexed with the scheelite structure. Some weaker new peaks, marked with an arrow, can be attributed to an admixture of a monazite phase. From

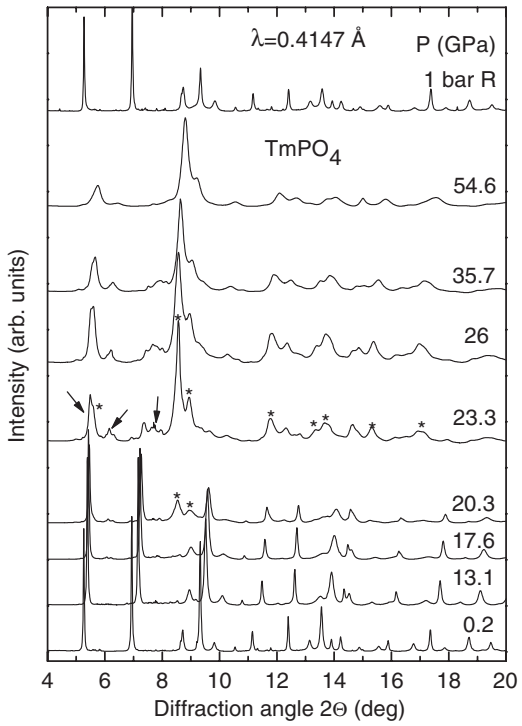

FIG. 2. X-ray diffraction patterns of $TmPO_4$ at various pressures. The asterisks and arrows denote Bragg peaks attributed to the scheelite and monazite phases, respectively.

relative intensities, it is estimated that just above the onset of the transition (∼23 GPa), the admixture of the monazite phase is merely about 10%. With increasing pressure, the monazite peaks gradually decrease in intensity and eventually vanish at a pressure of about 47 GPa. These observations indicate the initial coexistence of a small admixture of a monazite phase to the dominant scheelite modification.

Upon pressure release, the scheelite phase is retained down to at least 11 GPa, well below the transition pressure upon upstroke and without any trace of monazite reappearing. Eventually, $TmPO_4$ reverses to its initial zircon-type structure (Fig. 2) at a pressure somewhere between 11 and 6 GPa. So, the zircon-to-scheelite transition displays considerable pressure hysteresis. The thermodynamic zircon-scheelite equilibrium pressure should fall into the middle of the hysteresis interval, which is about 15 GPa.

The diffraction patterns were analyzed by performing Rietveld refinements using the GSAS (Ref. 23) software. Typical refined profiles are shown in Fig. 3 for (a) 13.1 GPa, zircon structure; (b) 26 GPa, mixture of scheelite and monazite; and (c) 54.6 GPa, scheelite. Comments are as follows: (1) Atom positional parameters were determined for the zircon phase through the full pressure range from ambient pressure up to 23 GPa. Representative results of full refinements for the zircon phase are given in Table I. (2) Attempts to fully refine the scheelite patterns led to unreasonable short bond lengths, something that has gone unnoticed in the work of Zhang *et al.*.[15] In our case, the reason in part is thought to be the major peak broadening after the phase transition. So, the positional parameters of scheelite-type YVO_4 (Ref. 24) were adopted in the refinements for the scheelite phase.

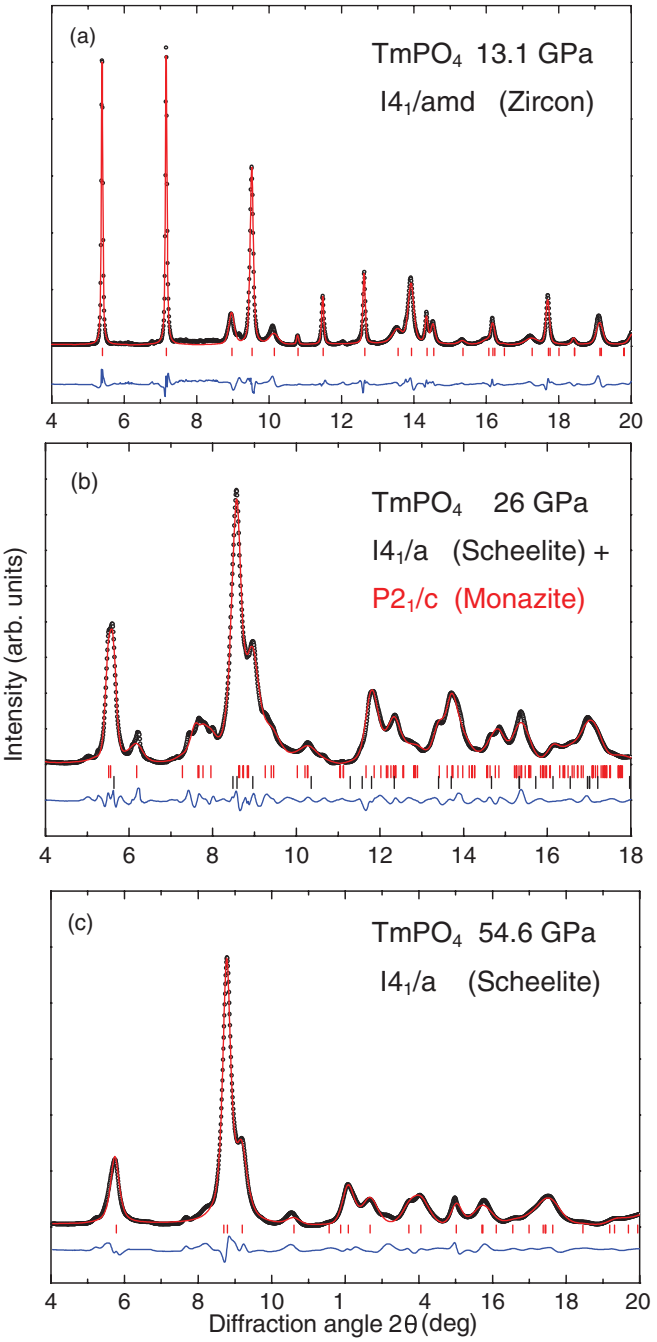

FIG. 3. (Color online) Rietveld refinements for $TmPO_4$ at (a) 13.1 GPa, zircon structure; (b) 26 GPa, mixture of scheelite and monazite; and (c) 54.6 GPa, scheelite.

The lattice parameters for the zircon and scheelite phases as a function of pressure (compression run only) are shown in Fig. 4. A small increase with pressure of the c/a ratio of the zircon phase is observed amounting to ∼1% over the pressure range up to the transition, whereas an equally small decrease of this ratio is seen for the scheelite phase in the range 20–55 GPa (Fig. 4).

The unit-cell volumes are shown in Fig. 5. There, the volume for the small monazite admixture is also indicated. The lattice parameters of monazite were determined by up to 8 Bragg peaks (011, 101, 200, 020, 111, 002, 130, 131),

TABLE I. Structural parameters of zircon-type $TmPO_4$ (SG I41/amd, No. 141) at three selected pressures: lattice parameters, unit-cell volume, and coordinates for oxygen in the 16*h* Wyckoff site. The standard deviations of the refinements are given in parentheses. The special positions for the cations are Tm in 4*a* (0, 3/4, 1/8) and P in 4*b* (0, 1/4, 3/8). The number of formula units in the conventional cell is $Z = 4$.

	0.2 GPa	13.1 GPa	20.3 GPa
a (Å)	6.835(1)	6.639(2)	6.538(3)
c (Å)	5.980(1)	5.907(3)	5.857(3)
V_{cell}	279.37(1)	260.39(3)	250.45(7)
x	0	0	0
y	0.9503(5)	0.9522(6)	0.9562(9)
z	0.7715(5)	0.7728(7)	0.7754(9)

not overlapping significantly with scheelite peaks positions. Nevertheless, the monazite cell volume comes with a relatively large uncertainty. The lattice parameters for monazite-type phase at 26 GPa are $a = 6.316$ Å, $b = 5.960$ Å, $c = 6.422$ Å, and $\beta = 104.35°$. The volume reduction at the zircon-to-scheelite transition is -8.8%. For the zircon-to-monazite transition, it is only about -3.1%.

In Table II, we summarize experimental structural parameters at selected pressures (including zero pressure) for the zircon- and scheelite-type phases. The ambient-pressure

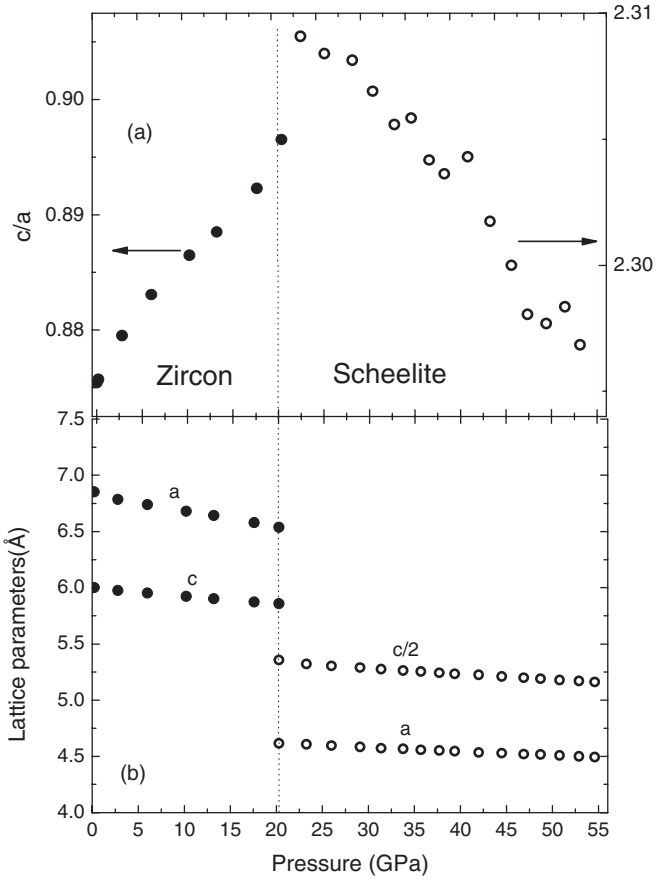

FIG. 4. Axial ratio and lattice constants for the zircon and scheelite phases of $TmPO_4$ as a function of pressure.

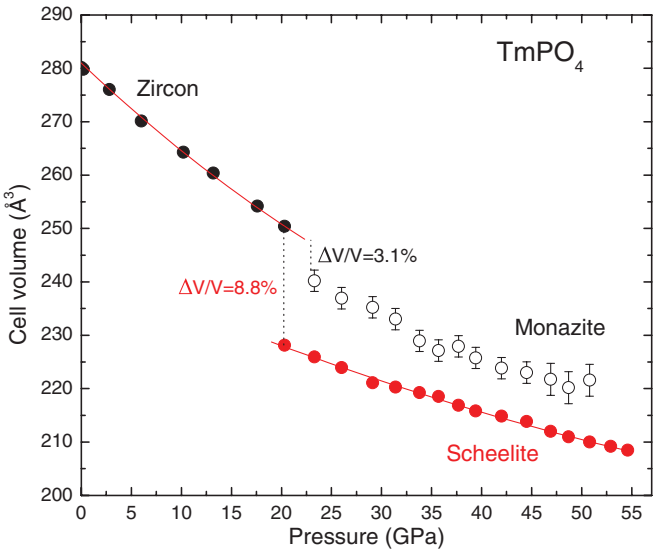

FIG. 5. (Color online) Volume-pressure data for the zircon, monazite, and scheelite phases of $TmPO_4$.

lattice parameters of the zircon phase are in full agreement with reported structural data[7] for $TmPO_4$. We have simulated the pressure-volume data by the third-order Birch equation of state[25] and determined the bulk modulus B and its first derivative B' for the zircon phase at zero pressure and the scheelite phase at 20.3 GPa. The corresponding values are given in Table II. It is perhaps noteworthy that the bulk modulus of $TmPO_4$ more than doubles (135 GPa $\rightarrow$ 291 GPa) between ambient pressure (zircon phase) and 20.3 GPa (scheelite), an increase which is larger than for any other orthophosphate[13,15] or orthovanadate[24,26,27] compound undergoing this transition.

A close inspection of the x-ray diffraction diagrams for the zircon-type phase of $TmPO_4$ shows an overall increase with pressure of the linewidths of Bragg peaks by a factor of 2, despite the fact that helium was used as a pressure-transmitting medium and the fraction of the gasket hole filled by the sample was less than 15% in projection. It is not clear whether this effect arises from local strains caused by touching grains or whether it is an intrinsic property of $TmPO_4$ related to the pronounced phonon anomaly revealed by our lattice-dynamics calculations (see the following).

C. Raman spectra

1. Ambient-pressure spectra

In order to work out the symmetry assignment of the Raman-active modes of zircon-type $TmPO_4$, we have examined a selection of ambient conditions Raman spectra of this compound recorded at various polarization configurations.

The symmetries and atomic displacements corresponding to the normal modes of the zircon-type structure are well established.[28] Twelve Raman-active zone-center modes are predicted[28] with the symmetries $2A_{1g} + 4B_{1g} + B_{2g} + 5E_g$; the E_g modes are doubly degenerate. Of these modes, seven $(2A_{1g} + 2B_{1g} + B_{2g} + 2E_g)$ can be considered internal, arising from vibrations of oxygen atoms in the $(PO_4)^{3-}$ tetrahedra, four $(2B_{1g} + 2E_g)$ are categorized as external brought about by relative translations of $(PO_4)^{3-}$ and Tm^{3+} ions, and one

TABLE II. Experimental and *ab initio* calculated lattice parameters a and c and cell volumes for the low- and high-pressure phases of $TmPO_4$ at selected pressures. Also given are bulk modulus B and its pressure derivative B' at zero pressure and at the experimental onset pressure for the scheelite phase.

Phase	P (GPa)		a (Å)	c (Å)	V (Å^3)	B (GPa)	B'
Zircon	0.0	Expt.	6.853(1)	5.989(1)	281.26(1)	135(1)	4.7(7)
	0.0	Calc.	6.87	5.99	284	140	5.3
	14.7	Expt.	6.624(2)	5.903(2)	257.34(4)		
	14.7	Calc.	6.66	5.89	261.2		
Scheelite	0	Calc.	4.804	11.134	257.3	163	4.3
	16.4	Calc.	4.69	10.73	237		
	20.3	Expt.	4.614(2)	10.782(3)	228.52(6)	291(5)	5.4(9)
	27.2	Expt.	4.606(3)	10.615(3)	222.45		
	27.2	Calc.	4.66	10.56	229.3		

(E_g) is attributed to rotations of $(PO_4)^{3-}$ tetrahedra units (see also Table III for mode assignments).

Polarized Raman spectra of $TmPO_4$ at ambient conditions are shown in Fig. 6. They were measured in $y(zz)x$, $z(xx)y$, $z(yx)y$, and $z(yz)y$ settings (Porto notation[29]), giving A_{1g}, $(A_{1g} + B_{1g})$, B_{2g}, and E_g symmetry modes, respectively (see also Ref. 10). Hereafter, these spectral components will be referred to by the symbols inside the brackets, which represent the polarizations of incident and scattered light. In the zz spectrum, the two strong Raman peaks at 488 and 1006 cm^{-1} (Fig. 6) are properly assigned as the two A_{1g} modes. Other weak peaks in the zz component constitute polarization leaks of other symmetry modes. In the yx spectrum, a strong sharp peak at 330 cm^{-1} is assigned as the sole B_{2g} mode; other weak peaks at high frequencies are due to polarization leaks from different components. Both A_{1g} and B_{1g} symmetry modes are expected in the xx spectrum, and apart from the strong peaks at 488 and 1006 cm^{-1}, which have already been assigned as A_{1g} modes, the other three strong peaks of this spectrum at 138, 660, and 1064 cm^{-1} are appropriately assigned as B_{1g} modes. Finally, in the yz spectrum (Fig. 6), several peaks appear, but if we exclude leaking from other components (already assigned), there are five peaks remaining at 132, 185, 303, 580, and 1027 cm^{-1}, which are accordingly assigned as the five E_g modes of the crystal. Therefore, we observe 11 out of 12 modes expected for the zircon-type phase. The 12th Raman mode (of B_{1g} symmetry) is not evident in our spectra; presumably, it is too weak for detection.

The mode frequencies at ambient conditions and their assignments obtained from polarized Raman spectroscopy are presented in Table III. In the table, we also give the character (internal/external) of the observed modes in accordance with previous relevant works.[28,30,31] Our measured frequencies are in excellent agreement with those observed in previous Raman studies[30,32] of $TmPO_4$ at ambient conditions. Our mode assignment differs partially from those reported previously

TABLE III. Assignments, ambient conditions, experimental and *ab initio* calculated frequencies ω_0, and experimental slopes $(\partial\omega/\partial P)_T$ of Raman modes of zircon-type $TmPO_4$ in combination with assignments, starting frequencies ω_0, and slopes of scheelite-type $TmPO_4$. The experimental and theoretical data for the scheelite phase refer to pressures of 20.5 and 16.4 GPa, respectively. Mode assignments for the zircon structure are based on both experimental and calculated data of this work, while those of the scheelite phase are heavily based on the calculated results. The symbols in parentheses in the mode assignments of zircon structure denote external translational (E), rotational (R) and internal (I) vibrational [in the $(PO_4)^{3-}$ units] modes, and are after Refs. 28,30, and 31.

	Zircon				Scheelite		
Assignment	ω_0 (expt.) (cm^{-1})	ω_0 (calc.) (cm^{-1})	$(\partial\omega/\partial P)_T$ (cm^{-1}GPa^{-1})	Assignment	ω_0 (expt.) (cm^{-1})	ω_0 (calc.) (cm^{-1})	$(\partial\omega/\partial P)_T$ (cm^{-1}GPa^{-1})
$E_g(E)$	132	129	0.22 ± 0.02	E_g	140	130	0.9 ± 0.1
$B_{1g}(E)$	138	136	0.85 ± 0.03	B_g		168	
$E_g(E)$	185	183	-0.01 ± 0.01	E_g		263	
$B_{1g}(E)$		286		A_g	305	296	0.6 ± 0.1
$E_g(R)$	303	303	4.35 ± 0.02	B_g	325	318	1.7 ± 0.2
$B_{2g}(I)$	330	314	-0.56 ± 0.02	E_g	420	403	0.1 ± 0.1
$A_{1g}(I)$	488	467	1.22 ± 0.04	A_g	470	440	0.6 ± 0.2
$E_g(I)$	580	554	0.99 ± 0.02	B_g	510	486	2.5 ± 0.2
$B_{1g}(I)$	660	630	1.99 ± 0.04		552		2.1 ± 0.2
$A_{1g}(I)$	1006	956	5.0 ± 0.1	E_g	635	595	1.6 ± 0.3
$E_g(I)$	1027	980	4.1 ± 0.1	B_g	661	600	1.2 ± 0.2
$B_{1g}(I)$	1064	1021	5.2 ± 0.1	A_g	1028	960	2.0 ± 0.4
				E_g	1060	1012	1.6 ± 0.5
				B_g	1089	1020	1.2 ± 0.7

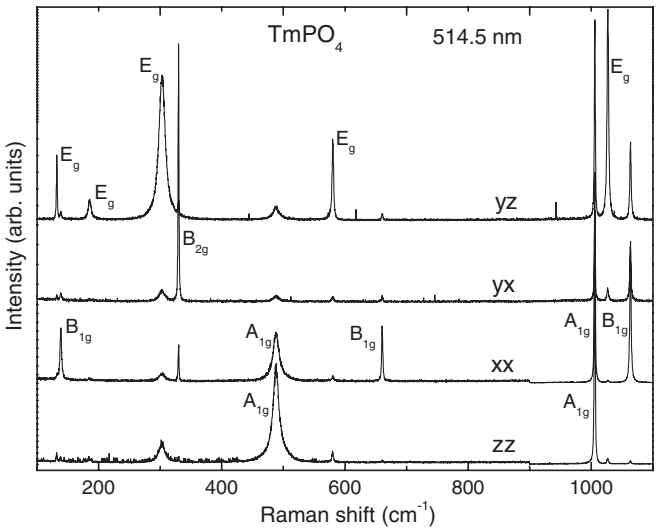

FIG. 6. Polarized Raman spectra of $TmPO_4$ at ambient conditions. The intensity scales of all four spectra are the same up to 900 cm^{-1}, but above this frequency, the zz and xx components have been suppressed by a factor of 5, for clarity.

for the three lowest-frequency external modes[30] and two high-frequency internal modes.[32] On the other hand, the mode assignments given in Table III are fully supported by the results of our *ab initio* calculations (see later). Also, the calculations predict that the nonobserved B_{1g} Raman mode has a frequency near 286 cm^{-1}.

2. *Raman modes under pressure*

Figure 7 shows a number of nonpolarized Raman spectra of single-crystal $TmPO_4$ at selected pressures up to 24 GPa for both compression and decompression runs. As in the ambient-pressure spectra, the same 11 Raman peaks of the zircon phase of $TmPO_4$ are seen when scattering takes place inside the DAC. Plots of frequency versus pressure for all observed modes of $TmPO_4$ are presented in Fig. 8 for the compression run. The pressure dependence of the B_{2g} bending mode follows a pattern similar to that observed in the isomorphous $TbPO_4$, i.e., it softens with pressure to an extent that a crossing occurs (Figs. 7 and 8) with the nearby E_g mode at 303 cm^{-1}, which hardens strongly with increasing pressure.

Most zircon-phase Raman peaks are clearly observed up to a pressure of 19.4 GPa. At 17.4 GPa, new Raman bands start to appear (Fig. 7), coexisting with bands of the zircon phase. The spectral changes seen at this pressure indicate the onset of a structural phase transition, which is almost completed at a pressure $P_c = 20.5$ GPa (Fig. 7). Above this pressure, 12 Raman peaks are observed. The number of observed Raman modes and the overall spectral shape of the spectra are compatible with the scheelite-type structure if compared to related reports.[33,34] So, the Raman measurements indicate a mixed zircon–scheelite phase in the range 17.4–20.5 GPa.

When compared with the diffraction data, the onset pressure of the phase transition is somewhat lower. This effect possibly results from nonhydrostatic stress present in the ethanol-methanol pressure medium above its solidification pressure (∼10 GPa); nonhydrostaticity tends to initiate a first-order

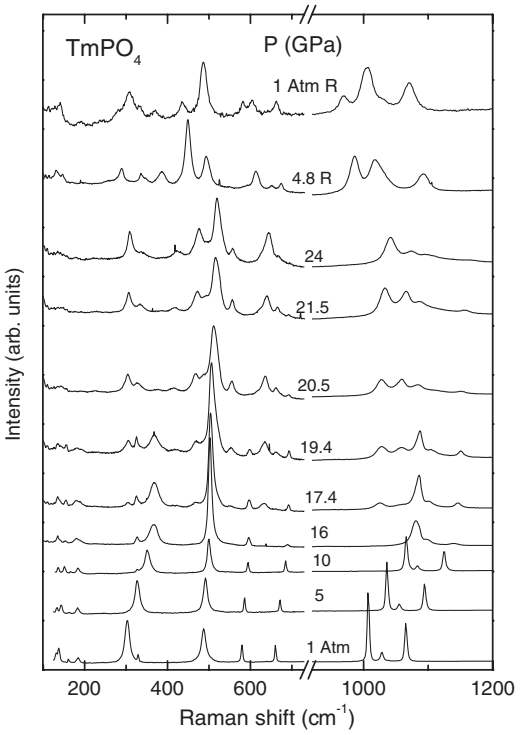

FIG. 7. Raman spectra of $TmPO_4$ at various pressures for both a compression and decompression sequence.

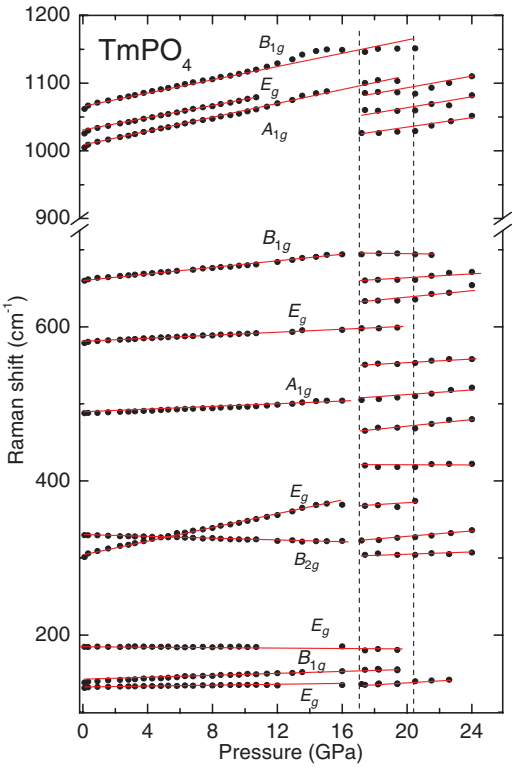

FIG. 8. (Color online) Frequencies of Raman modes against pressure for the compression run, showing two critical pressure values at 17.4 GPa (onset of the zircon-to-scheelite transition) and 20.5 GPa (completion of transition). The solid lines are results of linear regressions.

transition at a pressure that is closer to the thermodynamic equilibrium pressure.

Group theory predicts 13 Raman-active modes for the scheelite structure with the following symmetries: $3A_g + 5B_g + 5E_g$. Mode correlations for the zircon-to-scheelite transition[35] imply that A_{1g} and B_{1g} (B_{2g}) symmetry modes of the zircon phase become A_g and B_g ones, respectively, in the scheelite structure, while the E_g maintain their symmetry. The additional 13th mode of the scheelite structure results from the activation of the A_{2g} silent mode of the zircon-type structure that transforms to a Raman-active A_g mode. In the high-pressure phase of $TmPO_4$, we observe 12 Raman peaks. Of these, 11 peaks can be matched to Raman modes of the scheelite-type structure as implied by our *ab initio* calculations. Comparison with the Raman spectra of other scheelite-type compounds[36,37] and with our calculated frequencies for the high-pressure phase shows that the two Raman bands, which are missing from our spectra, correspond to low-frequency B_g and E_g external modes.

The mode frequencies obtained from our Raman measurements for the high-pressure scheelite phase of $TmPO_4$ are given in Table III, along with the respective experimental pressure coefficients. Also listed in Table III are the results of our *ab initio* calculations, which provide the mode assignments for the scheelite phase. We notice a good overall agreement between experimental and calculated frequency values. One notable discrepancy is for the peak observed at 552 cm^{-1} (20.5 GPa). The calculations do not account for the frequency of this peak, so its origin is ambiguous. It may be due to a strong Raman mode of the monazite structure, which is known from our x-ray data to form as a companion metastable phase. However, considering the small proportion (∼10%) in which this phase is formed, its tracing by Raman scattering looks rather unrealistic.

The decompression cycle in the Raman experiments indicates that $TmPO_4$ reverses only partially to its stable ambient-pressure structure. Raman peaks of the zircon phase (Fig. 7) reappear in the spectrum as the crystal is quenched down to ambient pressure, with the positions of peaks coinciding with those of the Raman bands prior to pressure application. However, the spectrum of the quenched crystal retains some bands of the high-pressure scheelite phase, even after a time lapse of 24 h.

Figure 9 shows the pressure dependence of the observed modes of the high-pressure scheelite phase for both compression and decompression, as well as that of zircon-phase modes, which reappear during the downstroke run. Different from the powder x-ray diffraction measurements, the Raman experiments, which start with a bulk single crystal, reveal a larger hysteresis upon pressure release, with the quenched material consisting of a mixed zircon–scheelite phase. We note that the broadening sustained by the Raman bands of $TmPO_4$ at the pressure-induced phase transition upon upstroke (Fig. 7) persists upon quenching to zero-pressure volume.

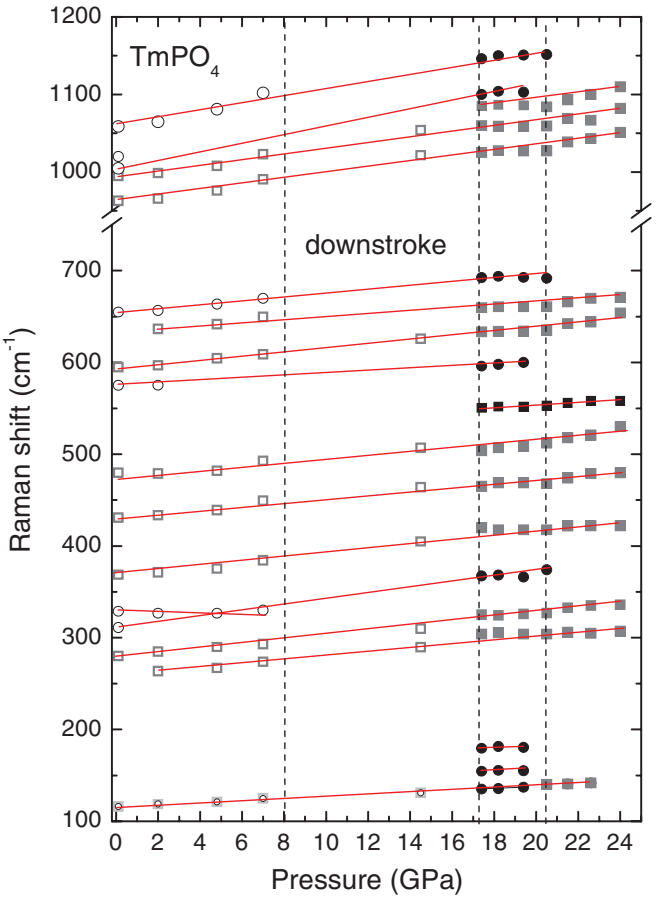

FIG. 9. (Color online) Frequencies of Raman modes of $TmPO_4$ for the zircon and scheelite phases above 17 GPa on upstroke (closed circles and squares, respectively) and for the downstroke (open symbols). The solid lines indicate results of linear regressions.

III. CALCULATIONS

A. Methods and approximations

The *ab initio* simulations reported here have been performed within the density functional theory (DFT) framework as implemented in the Vienna *ab initio* simulation package (VASP) (see Refs. 38 and 39 and references therein). The package performs *ab initio* electronic-structure calculations with the plane-wave pseudopotential method. The set of plane waves employed extended up to a kinetic energy cutoff of 550 eV; such a large cutoff was required to achieve highly converged results within the projector-augmented-wave (PAW) scheme.[39,40] The PAW method takes into account the full nodal character of the all-electron charge density distribution in the core region. It is known that standard DFT does not work properly for strongly localized f electrons. To deal with this problem, we adopted the standard procedure to treat the f electrons using a PAW pseudopotential.[41,42] For the Tm atom, all the f electrons except one are frozen in the core during the pseudopotential generation. The exchange-correlation energy was taken in the generalized gradient approximation (GGA) with the Perdew-Burke-Ernzerhof (PBE) prescription;[43] it is well known that the GGA approach underestimates the cohesion energy[44] (in turn producing an overestimation of the equilibrium volume). We used dense special point grids appropriate to each structure considered to sample the Brillouin zone (BZ), thus ensuring a high convergence of 1–2 meV per formula unit in the total energy of each structure as well as an accurate calculation of the forces over the atoms. At each selected volume, the structures were

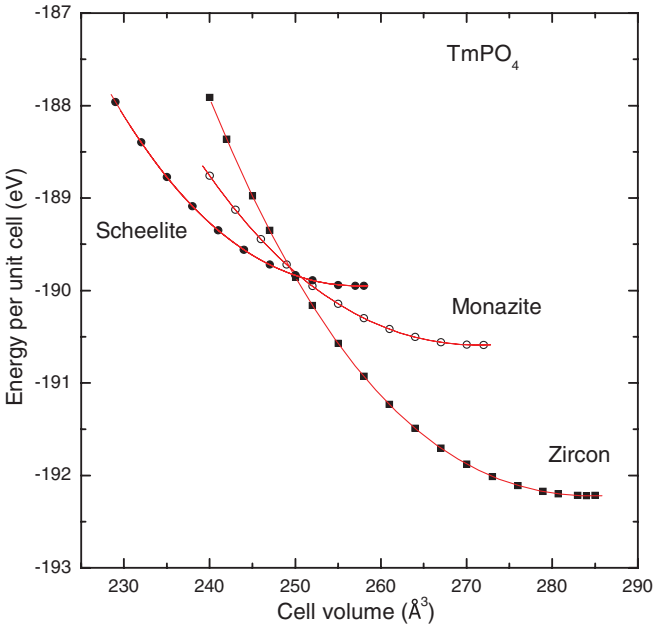

FIG. 10. (Color online) Calculated total energy for the zircon, scheelite, and monazite phases of $TmPO_4$ plotted against cell volume.

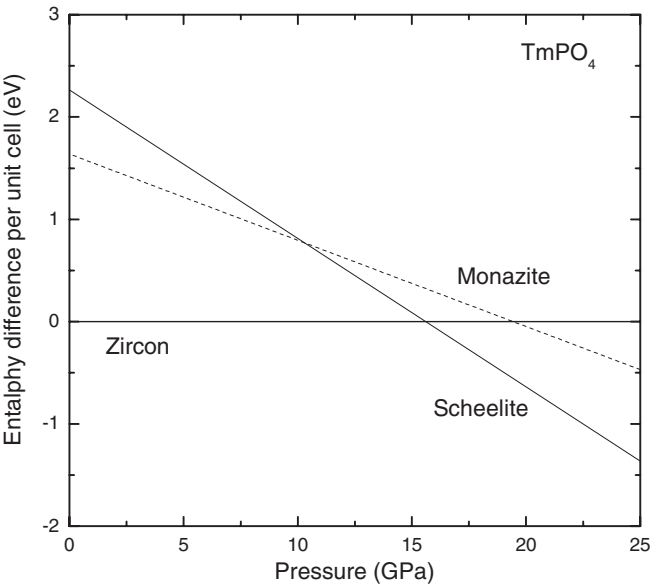

FIG. 11. Calculated enthalpy differences for the zircon, scheelite, and monazite phases of $TmPO_4$ as a function of pressure. The enthalpy of the zircon phase is taken as reference.

fully relaxed to their equilibrium configurations through the calculation of the forces on atoms and the stress tensor.[44] In the relaxed equilibrium configuration, the forces were smaller than 0.004 eV/Å, and the deviation of the stress tensor from a diagonal hydrostatic form was less than 1–2 kbar.

Lattice-dynamic calculations of phonon modes were performed in zircon and scheelite structures at the zone center (Γ point) of the BZ. We used a direct force-constant approach (or supercell method).[45] These calculations provide information about the symmetry of the modes and their polarization vectors, and allowed us to identify the irreducible representations and the character of the phonon modes at the Γ point.

B. Total energy, enthalpy, and phase stability

In order to study theoretically the structural stability of $TmPO_4$ at high pressures we have considered, along with the zircon structure, two other structures with which APO_4 orthophosphates have been related recently[10–15] in pressure-induced phase transition studies, namely, the scheelite and monazite ones.

Figures 10 and 11 show plots of *ab initio* calculated total energy and enthalpy as functions of volume and pressure, respectively, for the three aforementioned structures. Both sets of plots clearly indicate that the zircon structure is stable at ambient and low pressures, while the high-pressure stable phase is that of scheelite. Also, from the crossing of the curves in Fig. 11, it is concluded that the transition from zircon to scheelite takes place at $P_c = 16.4$ GPa. However, it is pointed out that in both Figs. 10 and 11, the total-energy and enthalpy values of the monazite structure around P_c are very close to the respective crossing values. The proximity of calculated values at P_c is quite important for interpreting the parallel formation of the monazite phase along with the scheelite one at high pressures [see the x-ray diffraction patterns of Figs. 2 and 3(b)].

C. Structural and elastic parameters

Structural parameter calculations have been performed up to 27 GPa, and the results for the cell volume as a function of pressure are shown in Fig. 12 for the three phases: zircon, scheelite, and monazite. From these calculations, a volume reduction of about 9% is obtained for the zircon-to-scheelite transition (16.4 GPa), which is in excellent agreement with the x-ray data (Fig. 5). Further, the calculated volume reduction for a zircon-to-monazite transition at 20 GPa amounts to about 5% (Fig. 12), in good agreement with the respective diffraction results (Fig. 5). The calculated lattice parameters a and c for the zircon and scheelite phases, and equilibrium volume V for the three structures at selected pressures shown in Table II, are

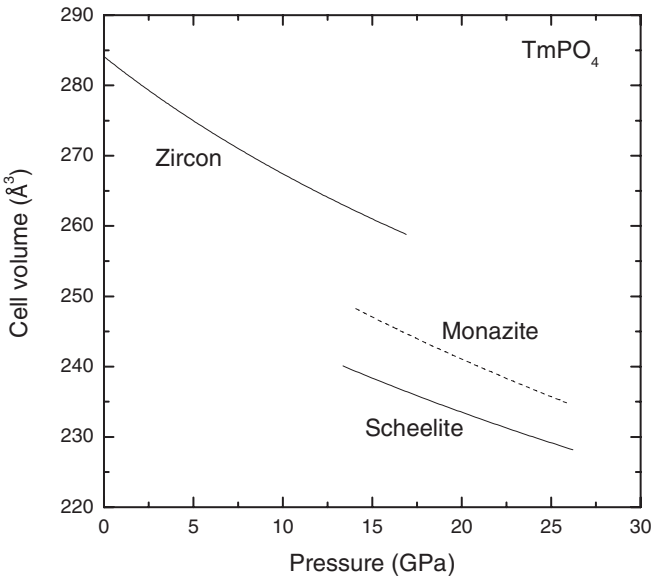

FIG. 12. Calculated cell volume of zircon, scheelite, and monazite phases of $TmPO_4$ plotted against pressure.

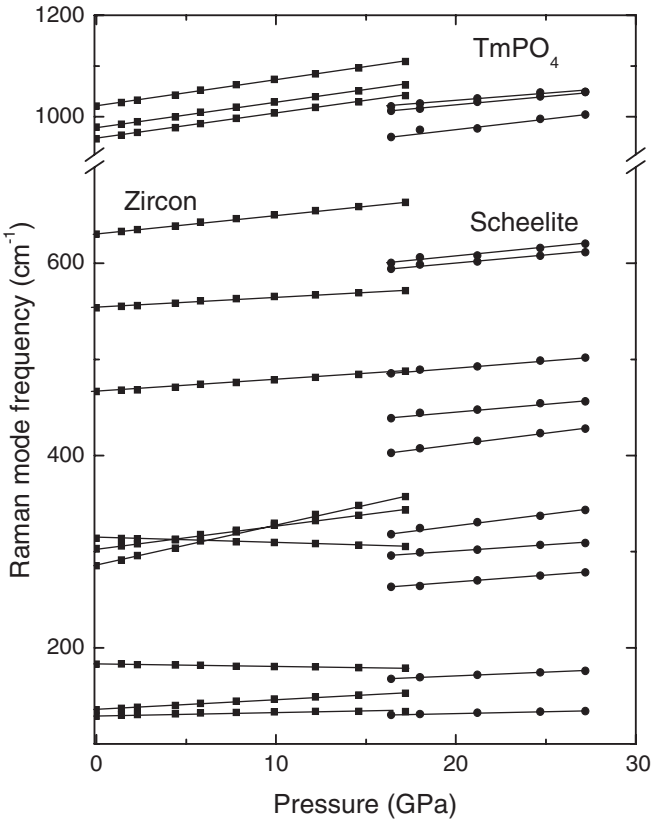

FIG. 13. Calculated frequencies of Raman modes of $TmPO_4$ as a function of pressure for the zircon and scheelite phases.

in good overall agreement with the experimentally obtained ones. The calculated energy-volume data have been fitted by a Birch equation of state[25] from which the calculated values of bulk modulus B and its pressure derivative B' at zero pressure have been obtained for the zircon and scheelite phases (see Table II). Note that the B and B' values given for the scheelite phase correspond to its calculated zero pressure.

D. Lattice-dynamics calculations

We have conducted *ab initio* lattice-dynamics calculations on $TmPO_4$ based on the method described in Sec. III A. From these calculations, we have obtained the frequencies and pressure dependence of all normal modes in both zircon and scheelite phases. The calculated Raman frequencies are given in Table III together with the experimental ones. Figure 13 shows the pressure dependence of the calculated Raman frequencies for both zircon and scheelite phases. There is very good overall agreement between experimental and theoretical results of mode frequencies at the equilibrium volume for each phase (Table III) and of their pressure dependence (Figs. 8 and 13). As noted in in Sec. II C, the only difference between experimental and theoretical results has to do with the observed Raman peak of the high-pressure phase at 552 cm^{-1}, which is not predicted by theory for the scheelite phase.

We have performed calculations to determine the frequencies of other zone-center modes of $TmPO_4$ at various pressures. A notable feature is the strong pressure dependence of the B_{1u} silent mode at 125 cm^{-1} of the zircon phase. This mode,

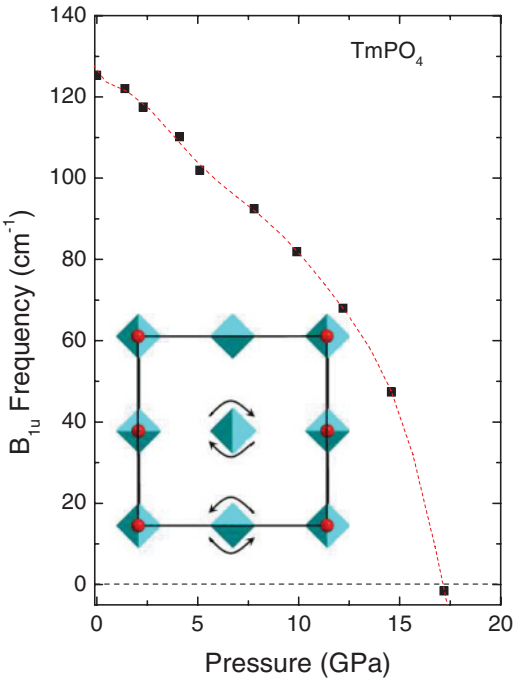

FIG. 14. (Color online) Calculated frequency of the B_{1u} silent mode of the zircon-type phase of $TmPO_4$ as a function of pressure.

which can be assigned[28] to rotations of rigid $(PO_4)^{3-}$ units and transforms[35] to an also silent B_u symmetry mode in the scheelite phase, is found to exhibit soft-mode behavior with pressure. At 17.4 GPa, its frequency becomes negative. A plot of calculated frequencies of this soft mode with pressure across the phase transition is given in Fig. 14.

IV. DISCUSSION

Both the x-ray diffraction patterns and Raman spectra confirm the zircon-type structure for $TmPO_4$ at ambient conditions. Assignment of all observed Raman modes of zircon-type $TmPO_4$ has been made by performing polarized measurements on an oriented single crystal, thus lifting the differences and ambiguities existing in the literature[30,32] about mode symmetries of this compound and generally of zircon-type orthophosphates.

The x-ray diffraction and Raman measurements, in combination with *ab initio* total-energy and lattice-dynamics calculations, clearly show that the high-pressure stable phase of $TmPO_4$ has the scheelite-type structure.

The diffraction patterns evidence the onset of the zircon-to-scheelite transition at about 20 GPa on upstroke. They also indicate the simultaneous formation of a monazite-type minority phase. Its admixture amounts to only ~10% at the phase transition, it decreases with pressure, and eventually vanishes at about 47 GPa. Unlike other scheelite-type ABO_4 compounds, which are known[5,37] to undergo a first- or second-order pressure-induced transition to the monoclinic M-fergusonite phase [SG: C_{2h}^6 $(I2/a)$, $Z = 4$], the scheelite-type $TmPO_4$ displays a relatively large stability range at high pressures, without any indication for a further transition or symmetry change being detected up to 55 GPa. Upon pressure release, the polycrystalline sample used in diffraction

experiments fully reverses to its starting zircon structure. The back-transformation to the zircon phase occurs between 6 and 11 GPa. So, there is significant hysteresis. Throughout the decompression process, no sign of the reappearance of the monazite phase has been detected.

As for elastic properties (Table III), we note that the bulk modulus of the scheelite phase at the phase transition (291 GPa) is more than twice the B_0 value of the zircon phase (135 GPa). This is a relatively large increase of stiffness among ABO_4 orthophosphates[12–15] and orthovanadates[5,24,27] undergoing a zircon-to-scheelite phase transition.

The changes observed in the Raman spectra of $TmPO_4$ at and above 17.4 GPa (Fig. 7) are in line with the zircon-to-scheelite transition evidenced by the diffraction data and are also supported by our total-energy calculations (Fig. 10). Both the number of the observed Raman peaks and their frequencies are consistent with scheelite being the high-pressure phase of $TmPO_4$. Compared to the diffraction experiments, the lower threshold for the phase transition observed in the Raman measurements (upstroke) is attributed to the presence of nonhydrostatic stresses in the pressure-transmitting medium. The presence of nonhydrostatic stresses tends to push the phase transition pressure closer to its thermodynamic equilibrium value. The use of a bulk single crystal in Raman possibly explains that the recovery path during decompression in the Raman experiments is somewhat different from what is seen on powder x-ray diffraction.

In the mode frequency versus pressure plots of Fig. 8, a discontinuous downshift is evident at the transition for the high-frequency modes near 1000 cm^{-1}. A related frequency lowering has also been observed in other ABO_4 compounds undergoing the zircon-to-monazite or zircon-to-scheelite transitions.[10,33,36,37] The high-frequency modes are due to vibrations of oxygen atoms in the $(PO_4)^{3-}$ tetrahedra. Since the nominal coordination count of phosphorous by oxygen remains unchanged at the transition, the lowering of frequencies rather reflects a change in the coordination of PO_4 units by the rare-earth ions and related changes of P–O bond lengths and angles.

A moderately anomalous trend of the zircon phase is the softening of the B_{2g} bending mode ($\omega_0 = 330$ cm^{-1}) under pressure (Fig. 8), a feature that has also been observed in other zircon-type orthophosphate[10,11,13] and orthovanadate[33,36,37] compounds at high pressures. This trend is compatible with the anomalous softening of the shear elastic constant C_{66} of $TmPO_4$ at low temperatures.[16] Since this elastic constant is related with a B_{2g} lattice distortion, in order to verify the anomalous elastic distortion with temperature, we have performed[46] low-temperature (ambient-pressure) Raman measurements on $TmPO_4$. We have found that the B_{2g} Raman mode also exhibits a softening when decreasing temperature from 350 to 20 K, although the effect is quite small (-1 cm^{-1}). Bearing in mind that this mode is internal, we suggest that in both pressure-induced compression and thermal contraction, the bending (shear) displacements associated with this mode may result in some deformation of the PO_4 tetrahedra of the zircon phase.

From our calculations of phonon frequencies, it appears that the pressure-driven instability of the zircon-type phase is associated with the pronounced softening of the B_{1u} silent mode (Fig. 14). The mode corresponds to rotations of rigid $(PO_4)^{3-}$ units. The frequency of this mode ($\omega_0 = 125$ cm^{-1}) is found to turn negative at a pressure very close to the experimentally determined pressure of the phase transition. In the zircon-type phase, the PO_4 tetrahedra are aligned along the a and b axes (Fig. 1), whereas in the monazite and scheelite phases, they are rotated with respect to each other (and with respect to the axes). So, it is plausible to relate the softening of the B_{1u} mode with the instability of the zircon structure relative to a structure where the tetrahedra are rotated with respect to each other. Actually, a large softening of the B_{1u} silent mode was also reported for YVO_4, which transforms from zircon to scheelite at 7.5 GPa,[37] but its possible relation to the structural instability of zircon-type YVO_4 escaped attention.

The structural changes observed for $TmPO_4$ under pressure can be related to the known structural systematics and phase transition sequences in other zircon-type APO_4 orthophosphates and in their isomorphic AVO_4 orthovanadates. Recent high-pressure studies on zircon-type $TbPO_4$, YPO_4, and $ErPO_4$ have shown that these compounds undergo a first transition to the monazite-type structure.[10,12–14,47] Furthermore, a post-monazite transition to a scheelite modification has been reported for two of these compounds, based on *ab initio* calculations for $TbPO_4$ and on combined x-ray diffraction, Raman experiments, and *ab initio* calculations for YPO_4.[12,13,47] Thus, the transition sequence is zircon-monazite-scheelite. In contrast, the compounds $YbPO_4$, $LuPO_4$, and $ScPO_4$ undergo a direct transition to the scheelite phase.[13,15,47] All the above-mentioned pressure-induced phase transitions are summarized in the bar diagram Fig. 15. The diagram also includes phase transitions of $DyPO_4$. These are deduced from our preliminary Raman scattering experiments for pressures up to 40 GPa. The Raman spectra of $DyPO_4$ are consistent with a zircon-monazite-scheelite sequence of phase transitions. Details will be reported elsewhere.

The overall trends from Fig. 15 are that (i) the stability range of zircon increases with decreasing radius of the A^{3+} cation, (ii) a high-pressure monazite modification exists only for compounds with large A^{3+} radius, and (iii) compounds with small A^{3+} radius transform directly from zircon to scheelite. The instability pressure of zircon-type $TmPO_4$ fits into the general trend. As for the first high-pressure modification, $TmPO_4$ appears to be a borderline case. The main transition is to the scheelite phase. There is no intermediate single-phase monazite as in $TbPO_4$ and YPO_4, but monazite appears as an admixture to scheelite.

The trends discussed above are in accord with recent calculations of the pressure-temperature phase diagram of selected RPO_4 compounds.[19] The calculations start from a semiempirical interatomic potential. An interesting result is obtained for $TmPO_4$. The compound is proposed to follow a zircon-monazite-scheelite sequence above 300 K, but to transform directly from zircon to scheelite below 300 K. In the calculations, the dependence of phase boundaries on temperature arises from differences in vibrational entropy for the different phases. In view of these finite-temperature results, our observation of a monazite admixture at the transition to scheelite would not be surprising. What is more difficult to explain is the large pressure range over which the monazite admixture is seen in the diffraction diagrams. Perhaps, metastable

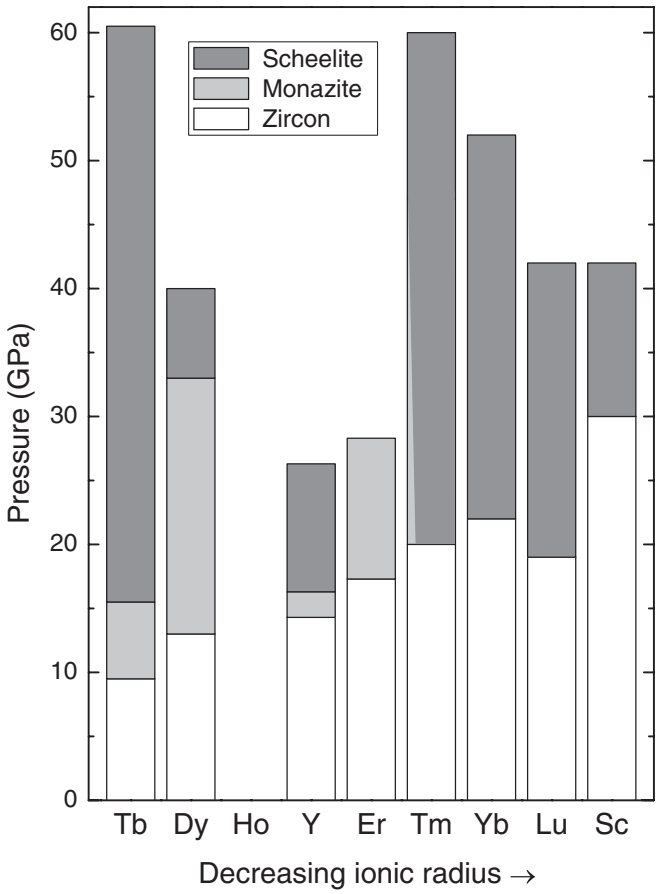

FIG. 15. Bar diagram showing the pressure stability intervals of the different structural modifications (zircon, monazite, and scheelite) of zircon-type orthophosphates. Critical pressures values are obtained with x-ray diffraction and/or Raman scattering measurements (see the references given in the text).

monazite grains are stabilized when embedded in a scheelite matrix.

A direct zircon-to-scheelite transition occurs in most zircon-type orthovanadates.[24,26,27,36,37,48] With the exception of $CeVO_4$, which displays the complete zircon-monazite-scheelite transition sequence,[49] all other zircon-type orthovanadates studied under pressure are known to undergo a direct transition to a scheelite-type phase. The different structural behavior under pressure of respective phosphates and vanadates can be understood in terms of the different stability and metastability fields[9] of the monazite (or zircon) phases for the two series of compounds.

V. SUMMARY

Results of x-ray diffraction and Raman measurements under pressure carried out on $TmPO_4$ are in good agreement with our *ab initio* calculations of structural stability and lattice-dynamical properties. Both the experimental methods and calculations show that the stable high-pressure phase of $TmPO_4$ above about 16–20 GPa is of the scheelite-type structure. Diffraction data indicate the appearance of a monazite-type metastable minority phase at the zircon-to-scheelite transition; the monazite fraction decreases when increasing pressure up to 47 GPa. The observed sequence of phase transitions in $TmPO_4$ is discussed in relation to the high-pressure behavior of isomorphic APO_4 and AVO_4 compounds. Our calculations indicate that the instability of the zircon-type phase of $TmPO_4$ may be related to a dramatic softening of a Raman-inactive B_{1u} mode. That mode corresponds to rotations of PO_4 tetrahedra. This type of mode softening could have relevance for the interpretation of the structural behavior of other zircon-type ABO_4 compounds under pressure. There are not many first-principles calculations for such compounds. This study points to what could be worthwhile to study in more detail.

ACKNOWLEDGMENTS

We would like to thank the materials preparation group of Clarendon Laboratory, University of Oxford, for providing a single-crystal sample of $TmPO_4$. A.M., J.L.-S. and P.R.-H. acknowledge the financial support of the Spanish MCIIN under Grants No. MAT2010-21270-C04/03 and No. CSD2007-00045, and the computer time provided by the Red Española de Supercomputación (RES).

*Present address: Technological Educational Institute of Epirus, Department of Communications, Informatics and Management, GR-47100 Arta, Greece.
†k.syassen@fkf.mpg.de

[1] O. Muller and R. Roy, *The Major Ternary Structural Families* (Springer, Berlin, 1974).
[2] O. Fukunaga and S. Yamaoka, Phys. Chem. Miner. **5**, 167 (1979).
[3] L. Liu and W. A. Bassett, *Elements, Oxides, Silicates: High-Pressure Phases with Implication for Earth's Interior* (Oxford Monographs on Geology and Geophysics, No. 4) (Oxford University Press, Oxford, UK, 1986).
[4] J. P. Bastide, J. Solid State Chem. **71**, 115 (1987).
[5] D. Errandonea and F. J. Manjon, Prog. Mater. Sci. **53**, 711 (2008).
[6] Y. X. Ni, J. M. Hughes, and A. N. Mariano, Am. Mineral. **80**, 21 (1995).
[7] A. Meldrum, L. A. Boatner, and R. C. Ewing, Phys. Rev. B **56**, 13805 (1997).
[8] S. V. Ushakov, K. B. Helean, A. Navrotsky, and L. A. Boatner, J. Mater. Res. **16**, 2623 (2001).
[9] U. Kolitsch and D. Holtstam, Eur. J. Mineral. **16**, 117 (2004).
[10] A. Tatsi, E. Stavrou, Y. C. Boulmetis, A. G. Kontos, Y. S. Raptis, and C. Raptis, J. Phys.: Condens. Matter **20**, 425216 (2008).
[11] E. Stavrou, A. Tatsi, E. Salpea, Y. C. Boulmetis, A. G. Kontos, Y. S. Raptis, and C. Raptis, J. Phys.: Conf. Ser. **121**, 042016 (2008).
[12] J. Lopez-Solano, P. Rodriguez-Hernandez, A. Muñoz, O. Gomis, D. Santamaria-Perez, D. Errandonea, F. J. Manjon, R. S. Kumar, E. Stavrou, and C. Raptis, Phys. Rev. B **81**, 144126 (2010).
[13] F. X. Zhang, J. W. Wang, M. Lang, J. M. Zhang, R. C. Ewing, and L. A. Boatner, Phys. Rev. B **80**, 184114 (2009).
[14] R. Lacomba-Perales, D. Errandonea, Y. Meng, and M. Bettinelli, Phys. Rev. B **81**, 064113 (2010).

[15]F. X. Zhang, M. Lang, R. C. Ewing, J. Lian, Z. W. Wang, J. Hu, and L. A. Boatner, J. Solid State Chem. **181**, 2633 (2008).
[16]R. T. Harley and D. I. Manning, J. Phys. C: Solid State Phys. **11**, L633 (1978).
[17]P. Morin, J. Rouchy, and Z. Kazei, J. Phys.: Condens. Matter **8**, 7967 (1996).
[18]W. Nagele, D. Hohlwein, and G. Domann, Z. Phys. B: Condens. Matter **39**, 305 (1980).
[19]P. P. Bose, R. Mittal, S. L. Chaplot, C. K. Loong, and L. A. Boatner, Phys. Rev. B **82**, 094309 (2010).
[20]B. M. Wanklyn, B. J. Garrard, and S. H. SmithH, J. Cryst. Growth **63**, 77 (1983).
[21]K. Syassen, High Pressure Res. **28**, 75 (2008).
[22]A. P. Hammersley, S. O. Svensson, M. Hanfland, A. N. Fitch, and D. Hausermann, High Pressure Res. **14**, 235 (1996).
[23]A. C. Larson and R. B. Von Dreele, General Structure Analysis System (GSAS), Los Alamos National Laboratory Report LAUR 86-748 (2004).
[24]X. Wang, I. Loa, K. Syassen, M. Hanfland, and B. Ferrand, Phys. Rev. B **70**, 064109 (2004).
[25]F. Birch, J. Geophys. Res. **83**, 1257 (1978).
[26]R. Mittal, A. B. Garg, V. Vijayakumar, S. N. Achary, A. K. Tyagi, B. K. Godwal, E. Busetto, A. Lausi, and S. L. Chaplot, J. Phys.: Condens. Matter **20**, 075223 (2008).
[27]D. Errandonea, R. Lacomba-Perales, J. Ruiz-Fuertes, A. Segura, S. N. Achary, and A. K. Tyagi, Phys. Rev. B **79**, 184104 (2009).
[28]P. Dawson, M. M. Hargreave, and G. R. Wilkinson, J. Phys. C: Solid State Phys. **4**, 240 (1971).
[29]S. P. S. Porto and R. S. Krishnan, J. Chem. Phys. **47**, 1009 (1967).
[30]G. M. Begun, W. B. G, L. A. Boatner, and W. J. Gregor, J. Raman Spectrosc. **11**, 273 (1981).
[31]R. J. Elliott, R. T. Harley, W. Hayes, and S. R. P. Smith, Proc. R. Soc. London **328**, 217 (1972).
[32]P. C. Becker, N. Edelstein, G. M. Williams, J. J. Bucher, R. E. Russo, J. A. Koningstein, L. A. Boatner, and M. M. Abraham, Phys. Rev. B **31**, 8102 (1985).
[33]S. J. Duclos, A. Jayaraman, G. P. Espinosa, A. S. Cooper, and R. G. Maines, J. Phys. Chem. Solids **50**, 769 (1989).
[34]E. Sarantopoulou, C. Raptis, S. Ves, D. Christofilos, and G. A. Kourouklis., J. Phys.: Condens. Matter **14**, 8925 (2002).
[35]D. L. Rousseau, R. P. Bauman, and S. P. S. Porto, J. Raman Spectrosc. **10**, 253 (1981).
[36]A. Jayaraman, G. A. Kourouklis, G. P. Espinosa, A. S. Cooper, and L. G. Vanuitert, J. Phys. Chem. Solids **48**, 755 (1987).
[37]F. J. Manjon, P. Rodriguez-Hernandez, A. Munoz, A. H. Romero, D. Errandonea, and K. Syassen, Phys. Rev. B **81**, 075202 (2010).
[38]G. Kresse and J. Furthmüller, Phys. Rev. B **54**, 11169 (1996).
[39]G. Kresse and D. Joubert, Phys. Rev. B **59**, 1758 (1999).
[40]P. E. Blochl, Phys. Rev. B **50**, 17953 (1994).
[41]J. Hafner, J. Comput. Chem. **29**, 2044 (2008).
[42]C. J. Pickard, B. Winkler, R. K. Chen, M. C. Payne, M. H. Lee, J. S. Lin, J. A. White, V. Milman, and D. Vanderbilt, Phys. Rev. Lett. **85**, 5122 (2000).
[43]J. P. Perdew, K. Burke, and M. Ernzerhof, Phys. Rev. Lett. **77**, 3865 (1996).
[44]A. Mujica, A. Rubio, A. Muñoz, and R. J. Needs, Rev. Mod. Phys. **75**, 863 (2003).
[45]K. Parlinski, computer code PHONON [http://wolf.ifj.edu.pl/phonon/].
[46]A. Tatsi, Ph.D. thesis, National Technical University of Athens, 2008.
[47]A. Mujica (private communication).
[48]J. Lopez-Solano, P. Rodriguez-Hernandez, and A. Muñoz, High Pressure Res. **29**, 582 (2009).
[49]K. J. Range, H. Meister, and U. Klement, Z. Naturforsch. B **45**, 598 (1990).